Received: 21 August 2019 | Revised: 4 December 2019 | Accepted: 24 December 2019

DOI: 10.1002/epi4.12379

FULL-LENGTH ORIGINAL RESEARCH

Epilepsia Open® Open Access

Persistent sodium current blockers can suppress seizures caused by loss of low-threshold D-type potassium currents: Predictions from an in silico study of K_v1 channel disorders

Jiaxin Du | **Viktor Vegh** | **David C. Reutens**

Centre for Advanced Imaging, The University of Queensland, St Lucia, Qld, Australia

Correspondence
Jiaxin Du, Centre for Advanced Imaging, University of Queensland, Building #57 Research Road, St Lucia, Qld 4072, Australia.
Email: j.du2@uq.edu.au

Funding information
Australian Research Council, Grant/Award Number: DP150104771

Abstract

Objective: Ion channels belonging to subfamily A of voltage-gated potassium channels (K_v1) are highly expressed on axons, where they play a key role in determining resting membrane potential, in shaping action potentials, and in modulating action potential frequency during repetitive neuronal firing. We aimed to study the genesis of seizures caused by mutations affecting K_v1 channels and searched for potential therapeutic targets.

Methods: We used a novel in silico model, the laminar cortex model (LCM), to examine changes in neuronal excitability and network dynamics associated with loss-of-function mutations in K_v1 channels. The LCM simulates the activities of a network of tens of thousands of interconnected neurons and incorporates the kinetics of 11 types of ion channel and three classes of neurotransmitter receptor. Changes in two types of potassium currents conducted by K_v1 channels were examined: slowly inactivating D-type currents and rapidly inactivating A-type currents. Effects on neuronal firing rate, action potential shape, and neuronal oscillation state were evaluated. A systematic parameter scan was performed to identify parameter changes that can reverse the effects of the changes.

Results: Reduced axonal D-type currents led to lower firing threshold and widened action potentials, both lowering the seizure threshold. Two potential therapeutic targets for treating seizures caused by loss-of-function changes in K_v1 channels were identified: persistent sodium channels and NMDA receptors. Blocking persistent sodium channels restored the firing threshold and reduced action potential width. NMDA receptor antagonists reduced excitatory postsynaptic currents from excessive glutamate release related to widened action potentials.

Significance: Riluzole reduces persistent sodium currents and excitatory postsynaptic currents from NMDA receptor activation. Our results suggest that this FDA-approved drug can be repurposed to treat epilepsies caused by mutations affecting axonal K_v1 channels.

KEYWORDS
genetic epilepsy, KCNA, LGI1, voltage-gated potassium channel

1 | INTRODUCTION

Voltage-gated potassium (K_v) channels are highly expressed in the brain.[1] They limit neuronal excitability by contributing to membrane repolarization and hyperpolarization. K_v1 channels are an important subgroup of the K_v family. They are primarily expressed on axons,[2] where they are responsible for determining resting membrane potentials, shaping action potentials, and modulating action potential (AP) frequency during repetitive neuronal firing.[3] Mutations in genes encoding K_v1 channels and related proteins cause several different epilepsy phenotypes. These genes include *LGI1*, *KCNA1*, and *KCNA2*, which encode the leucine-rich glioma-inactivated 1 protein, $K_v1.1$ and $K_v1.2$ channels, respectively. *LGI1* mutations are associated with autosomal dominant temporal lobe epilepsy, *KCNA1* mutations can cause episodic ataxia 1, usually associated with seizures, and both *KCNA1* and *KCNA2* mutations have been associated with epileptic encephalopathy. Associated epilepsy phenotypes can be refractory to existing antiepileptic medications, often with devastating sequelae. *LGI1* encodes a protein that regulates the expression and function of K_v1 channels and AMPA receptors.[4–10] In *LGI1* knockout models, the expression of $K_v1.1$ and $K_v1.2$ channels is reduced by more than 50%.[5] Depletion of leucine-rich glioma-inactivated 1 protein also increases the release of glutamate[10,11] and significantly reduces the expression of AMPA receptors.[6,8,9] These changes have mixed effects on the excitability of neurons, and the mechanisms by which *LGI1* mutations cause epilepsy remain elusive. $K_v1.1$ and $K_v1.2$ potassium channels activate rapidly at relatively low voltage (<−40 mV).[11] Most of these channels inactivate slowly and contribute to long-lasting D-type currents. However, when they co-assemble with $K_v1.4$ or auxiliary $K_v\beta1$ subunits, they display rapid inactivation, contributing to transient A-type currents. Hence, loss of $K_v1.1$ or $K_v1.2$ channels reduces both D-type and A-type currents.

In the present paper, we decided to study seizure genesis in epilepsies associated with loss-of-function mutations in K_v1 channels using computer simulations based on the laminar cortex model (LCM).[12,13] The LCM is a computational framework designed to simulate the activities of a thalamocortical network comprising tens of thousands of interconnected neurons. The model incorporates a realistic synaptic connection map, thalamocortical architecture, and 11 neuron types, with distinct action potential firing behaviors, into an integrated simulation framework. Neuron behaviors incorporate the kinetics of 11 types of ion channel as well as short-term synaptic plasticity. These features allow us to model the effects of changes in ion channel properties associated with gene defects realistically. We use the LCM to examine the effects of *KCNA1*, *KCNA2*, and *LGI1* mutations on neuronal excitability and network dynamics. To search for potential therapeutic targets, we performed a systematic parameter scan to identify those that can be tuned to reverse the effects of the gene mutations.

Key Points

- Reductions in axonal D-type currents and not in axonal A-type currents led to a lower firing threshold and wider action potentials.
- A 25-50 reduction in persistent sodium currents can compensate the neuronal changes caused by a 50 reduction in K_v1 channels.
- Seizure threshold decreases by >60 when D-type currents are halved; widening of action potentials lowered seizure threshold by ~30.
- Riluzole can reduce persistent sodium currents by ~25, which can restore the lowered seizure thresholds caused by K_v1 channel loss

2 | EXPERIMENTAL PROCEDURES

In this section, we briefly introduce the architecture of the LCM and outline the parameters used to describe ion channel kinetics.

2.1 | Ion channel kinetics

In the LCM, a neuron consists of several connected segments, which are modeled as a small cylindrical compartment with a set of ion channels (see Figure 1). The membrane potential of a segment is driven by ion channel currents and postsynaptic currents, stated as

$$C_{\mathrm{m,i}}\frac{\mathrm{d}V_{m,i}}{\mathrm{d}t} = -\sum\nolimits_{IC} g_{IC}(V_{m,i}-E_A) - \sum\nolimits_{sy} g_{sy}(V_{m,i}-E_{sy}) - \sum\nolimits_{j} g_{ij}(V_{m,i}-V_{m,j}), \quad (1)$$

where $V_{m,i}$ and $V_{m,j}$ are the membrane potentials of the segments i and j, respectively; $c_{\mathrm{m,i}} = C_m A_i$ is the *total* membrane capacitance for a segment with surface area A_i and specific membrane

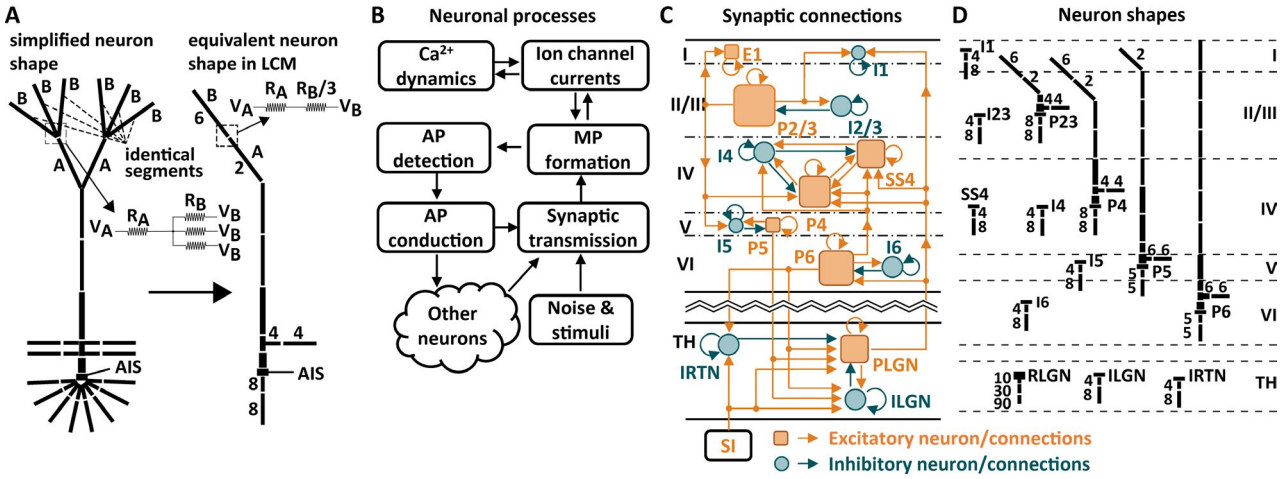

FIGURE 1 Architecture of the laminar cortex model (LCM). The sub-figures illustrate (A) a simplified shape for a pyramidal neuron and the equivalent representation in the LCM, (B) a flowchart of the neuronal processes modeled for a neuron in an iteration step, (C) synaptic connections between neuron classes, and (D) the equivalent shapes and laminar locations of the neuron classes modeled in the LCM. The numbers beside neuron segments in figure (A) and (D) indicate the weights of the segments. The weight is not shown for segments with a weight of 1. Acronyms: SI–sensory input; TH–thalamus; AP–action potential; PSP–postsynaptic potential; MP–membrane potential; E1–excitatory neurons in layer I of the cortex; I1–interneurons in layer I; P2/3–pyramidal neurons in layer II and III; I2/3–interneurons in layer II and III; P4–pyramidal neurons in layer IV; SS4–spiny stellate neurons in layer IV; I4–interneurons in layer IV; P5–pyramidal neurons in layer V; I5–interneurons in layer V; P6–pyramidal neurons in layer VI, I6–interneurons in layer VI; IRTN–interneurons in RTN of the thalamus; RLGN–relay neurons in LGN of the thalamus; ILGN–interneurons in LGN

capacitance C_m, and is set to 0.9 μF/cm^2;[14] g_{IC} is the *total* conductance of ion channel *IC*; E_A is the reversal potential of the corresponding ion; g_{sy} and E_{sy} are the *total* conductance and reversal potential of synapse *sy*, respectively; and g_{ij} is the intracellular conductance between segment *i* and *j*. The last summation in the right hand of Equation (1) is performed over all segments that are connected to segment *i*. The LCM simulates one type of leaking currents and eleven types of voltage-gated ion channel for three ion species (sodium, potassium, and calcium).[15] The kinetics of the ion channels are modeled using the Hodgkin-Huxley method. The currents passing through an ion channel are given by:

$$g = \bar{g} m^n h G, \tag{2}$$

where g is the temporally varying conductance, $\bar{g}$ is its peak conductance; $0 \le m, h \le 1$ are the activation and inactivation probabilities, respectively, with $h = 1$ for non-activating ion channels; n = 1, 2, 3, or 4 is the power of activation probability; $0 \le G \le 1$; is the gating probability, dependent on mechanisms other than membrane potential, and is set to 1 for ion channels that are only activated and inactivated by membrane potentials. The activation and inactivation probabilities are voltage-dependent, and follow the Hodgkin-Huxley first-order differential equations,

$$\frac{dm}{dt} = \frac{m^\infty - m}{\tau_m}, \frac{dh}{dt} = \frac{h^\infty - h}{\tau_h}, \tag{3}$$

where m^∞ and h^∞ are steady-state values, and τ_m and τ_h are time constants. Ion channels incorporated in the LCM and the notation for their conductance are listed below:

1. Leaking conductance (g_L, passive);
2. Sodium currents: (a) fast activating and inactivating transient conductance (g_{NaT}); (b) slowly activating and non-inactivating persistent conductance (g_{NaP});
3. Potassium currents: (a) low-voltage and fast-activating D-type conductance (g_{KD}); (b) fast activating and inactivating A-type transient conductance (g_{KA}); (c) Kv2 conductance by Kv2-like channels (g_{Kv2}); (d) Kv3.1 conductance by Kv3.1 like channels (g_{Kv3_1}); (e) muscarinic sensitive M-type conductance (g_{KM}); (f) intracellular calcium-dependent conductance (g_{SK});
4. Calcium currents: (a) low-threshold transient inactivating conductance (g_{CaLVA}); (b) high-threshold non-inactivating conductance (g_{CaHVA});
5. Non-selective anomalous rectifier (AR) conductance by the hyperpolarization-activated cyclic nucleotide-gated channels (g_{AR}).

The voltage dependence of the activation and inactivation probabilities is adopted from the work of Hay et al[16] and listed in the Supplementary Information (Figure S1 and Data S1).

An iteration equation of membrane potentials is drawn from Equation (1):

$$V_{m,i}(t_n + \Delta t) = V_{ss} - \left[V_{ss} - V_{m,i}(t_n)\right] \exp\left(-\Delta t_n / \tau_M\right) \tag{4}$$

where t_n is the time at iteration step n, Δt_n is the size of the iteration step, and V_{ss} and τ_M are the steady value and time constant of the membrane potential with values given by:

$$\tau_M = \frac{c_M}{\sum_{IC} g_{IC} + \sum_{sy} g_{sy} + \sum_{ij} g_{ij}},$$
$$V_{ss} = \frac{\sum_{IC} g_{IC} E_{IC} + \sum_{sy} g_{sy} E_{sy} + \sum_i g_{ij} V_{m,\mathrm{j}}}{\sum_{IC} g_{IC} + \sum_{sy} g_{sy} + \sum_i g_{ij}}. \quad (5)$$

In the LCM, Equations (4) and (5) are used to update membrane potentials of segments repetitively in discrete time steps. The LCM adopts variable time steps, and the size of an iteration step depends on the second-order derivative of membrane potential, $\Delta t = \sqrt{0.01/2V_m''}$. The time step is capped within 0.02 and 0.1 ms.

For calcium-dependent potassium currents ($g_{K(Ca)}$ and $g_{K(AHP)}$), the intracellular calcium concentration is modeled using.

$$\frac{\mathrm{d}[Ca^{2+}]_i}{\mathrm{d}t} = -\gamma i_{Ca} - [Ca^{2+}]_i/\tau_{Cai} \quad (6)$$

where i_{Ca} is the calcium current, γ is a coefficient characterizing concentration change caused by the currents, set to 0.002 μmol/L·cm^2/(ms·μA),[17] and τ_{Cai} is the ion concentration recovery time constant, set to 80 ms.[17]

2.2 | Synaptic transmission and short-term plasticity

Short-term synaptic plasticity of the PSC is incorporated into the model. Three types of neurotransmitter receptors are simulated: AMPA, NMDA, and GABAA. Postsynaptic currents triggered by a spike are given by:

$$I_{sy} = N_{sy}\, g_{sy}\, (V_{m,\,\mathrm{post}} - E_{sy})\, R(t) \quad (7)$$

where N_{sy} is the number of synapses, E_{sy} is the reverse potential, set to 0 mV for AMPA and NMDA receptors and to −80 mV for GABAA receptors, $R(t)$ is the time course of postsynaptic currents, modeled using a bi-exponential function (see Du et al[12]), and g_{sy} is temporally varied conductance of the receptors, determined using:

$$g_{sy} = \overline{g}_{sy}\, n_{sy}\, p_{sy} f\,(V_{\mathrm{m,\,post}}) \quad (8)$$

where $\overline{g}_{sy}$ is the peak conductance of a synapse, n_{sy} is the occupancy of the neurotransmitter pool in the presynaptic terminals and has a value between 0 and 1, p_{sy} is the portion of the neurotransmitter released upon the arrival of presynaptic spikes, $f(V_{m,\mathrm{post}})$, is a factor describing the PSC dependency on the membrane potential of the postsynaptic neurons ($V_{m,\mathrm{post}}$ see below). Occupancy of the neurotransmitter pool V_{sy} is reduced by presynaptic spikes and recovers with time and is described by:

$$\frac{\mathrm{d}n_{sy}}{\mathrm{d}t} = \frac{1 - n_{sy}}{\tau_{sy}} - \sum_j \delta(t - t_j) \cdot p_{sy} \cdot n_{sy}, \quad (9)$$

where τ_{sy} is the time constant characterizing the neurotransmitter pool recovery speed, $\delta(t\text{-}t_1)$ is the delta function, which is 1 when $t = t_j$ and 0 otherwise and t_j is the arrival time of presynaptic spikes. The conductance of AMPA and GABAA receptors is assumed to be dependent on postsynaptic membrane potential $V_{m,\mathrm{post}}$, (ie, $f(V_{m,\mathrm{post}})$ in Equation (7)), and the conductance of NMDA receptors has a sigmoidal relationship with $V_{m,\mathrm{post}}$, that is:

$$f(V_{\mathrm{m,\,post}}) = \frac{1}{1 + \exp\left[-(V_{\mathrm{m,\,post}} - \theta_{\mathrm{NMDA}})/k_{\mathrm{NMDA}}\right]} \quad (10)$$

with $\theta_{\mathrm{NMDA}} = -20.53$ mV and $k_{\mathrm{NMDA}} = 16.13$ mV[18].

2.3 | Local field potential computations

Local field potentials at the center of the stimulated cortical area are computed using:

$$LFP = \frac{1}{4\pi\sigma} \sum_i \frac{I_i}{r_i} \quad (11)$$

where σ is the conductivity of the cerebrospinal fluid, which is set to 1.56 S/m,[19] l_i are the total currents generated by a segment including leaking currents, ionic channel currents, and postsynaptic currents, r_i is the distance between the local field potentials (LFP) measurement location and the segment, and the summation runs over all the segments of all neurons in the model. The LFPs computed using Equation (11) are dominated by the activities of a small number of neurons around the electrode. To measure the overall network activity, we manually set r_i to 100 μm whether they are smaller than 100 μm.

2.4 | Computer simulation

The simulation program was written using the C++ language and compiled with the Intel C++ compiler (http://software.intel.com/intel-compilers/, version 19.03). The program was compiled and executed on the Tinaroo computing facilities provided by the Research Computing Center at the University of Queensland. OpenMP (http://www.openmp.org), a shared-memory parallel programming library, was used to parallelize the code to speed up program execution. The authors wish to provide the

program for the purpose of validating the results reported here.

3 | RESULTS

3.1 | Laminar cortex model with ion channel kinetics

The features of the LCM are summarized in Figure 1. A conductance-based model was used to simulate neuronal membrane potentials. The model incorporated the following ion currents: passive leaking currents (I_{Pas}), transient (I_{NaT}) and persistent (I_{NaP}) sodium currents, transient low-voltage activated T-type (I_{CaLVA}) and long-lasting high-voltage activated L-type (I_{CaHAV}) calcium currents, calcium-dependent potassium currents (I_{SK}), and the non-selective anomalous rectifier (I_{AR} or I_h), and five types of voltage-dependent potassium currents—slowly inactivating D-type currents (I_{KD}), transient rapidly inactivating A-type currents (I_{KA}, see below), M-type currents (I_{KM}), currents conducted by K_v2-like channels (I_{Kv2}) and by K_v3-like channels (I_{Kv3}). The ion channel activation and inactivation information for currents other than A-type currents were adopted from the publications of the Blue Brain Project.[16,20,21] We distinguish D-type currents conducted by K_v1 from those conducted by K_v2 and K_v3 channels, because D-type K_v1 channels activate at much lower voltage (~−43 mV) than K_v2 or K_v3 channels (~−20 and 18 mV, respectively) and inactivate at lower voltage (~−67 mV) than K_v2 channels (~−58 mV). Two types of A-type currents were modeled: axonal A-type currents conducted by rapidly inactivating K_v1 channels (I_{KA1}), and somatodendritic A-type currents conducted by K_v4 channels (I_{KA2}). Channel activation and inactivation data of the two A-type currents were drawn from the work of Roeper et al[22] and Mendonca et al[23] I_{KA1} activates at a higher voltage than I_{KA2}, and unlike I_{KA2}, I_{KA1} has two inactivation processes with time constants around 8 and 40 ms[22] The activation and inactivation thresholds and time constants of the ion channels are shown in Figure 2A, and additional details are provided in Supplementary Information (Figure S1 and Data S1).

A weighted segment model was used to reduce the computational complexity of iteratively updating membrane potentials. A segment in the LCM incorporates most of the features of the compartment model implemented in the NEURON platform,[24] including passive electrical properties, ion channel kinetics, and inter-segment conductance. Two additional features of each segment are a dendrite field and a weight factor. The dendrite field is a cylindrical space in which synapses are distributed around the segment. We assumed that the dendrites are purely passive, allowing their effects on postsynaptic currents to be modeled by an exponential decay function.[25] A segment may connect to several segments with identical biophysical properties. To avoid simulating multiple identical segments, we introduced a weight factor to the segment (see Figure 1A). This controls the conductances between segments so that a segment with a weight of n is equivalent to n identical segments when connecting to another segment (see Figure 1A and Supplementary Information Figure S1 and Data S1). The simplified neuron shapes used in the LCM are shown in Figure 1D.

Cortical neurons display several firing patterns, such as regular-spiking (RS), fast-spiking (FS), and intrinsic bursting

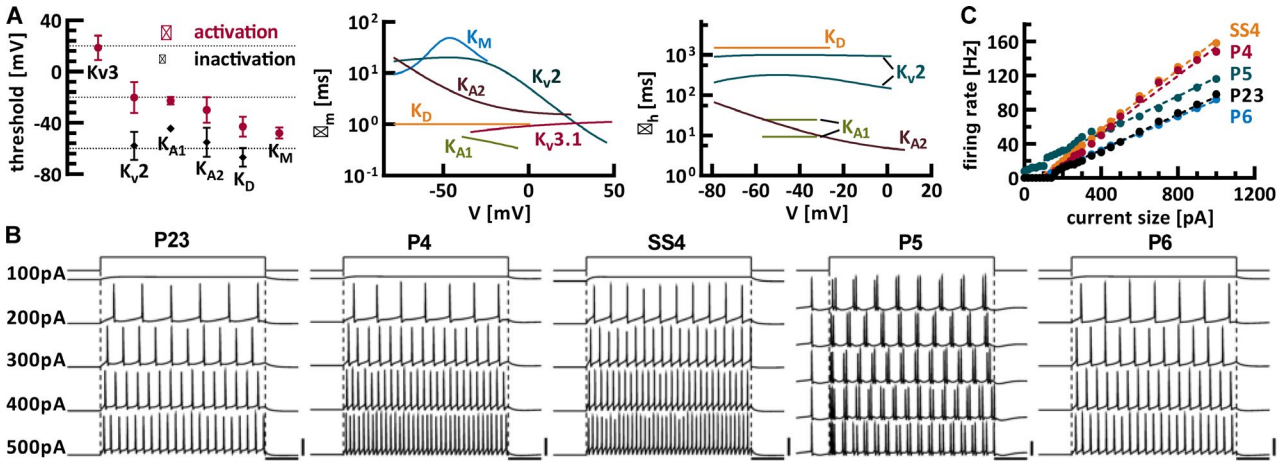

FIGURE 2 Ion channel activation and inactivation information and neuronal firing behaviors. Displayed are (A) the voltage dependency of activation and inactivation thresholds and time constants (τ_m, τ_h) for potassium channels, (B) the membrane potentials of the axon initial segment in five neuron classes during a 500-ms current injection into the soma, and (C) the relationships between firing rate and current size for the neurons. In (A), the markers and error bars indicate the respective values for $\theta_{m(h)}$ and $\sigma_{m(h)}$ in the Boltzmann function $m^{\infty} = 1/[1 + \exp[-(V-\theta_m)]/\sigma_m]$ or $h^{\infty} = 1/[1 + \exp[-(V-\theta_h)]/\sigma_h]$ used to describe the voltage dependence of ion channel activation and inactivation. In (B), the current sizes are shown on the left, the horizontal scale bars represent 100 ms, and the vertical scale bars represent 50 mV. See also Figure S1

(IB). To mimic these firing patterns, we configured each neuron class with a range of ion channel conductances and stimulated it with a 500-ms current injection into the soma. We tested a series of current amplitudes from 0 to 1000 pA to determine the relationship between neuronal firing rate and current amplitude (ie, F-I curve). We measured five quantities for each test: (a) the slope of the F-I curve, determined using a linear regression; (b) the firing rheobase, the minimum current required to elicit a spike; (c) inter-spike intervals (ISI), (d) AP height and (e) AP width at −20 mV. Typical firing behaviors and F-I relations of neurons are shown in Figure 2B,C. Firing behaviors aligned with experimental observations.[26–28]

3.2 | Impact of K_v1 loss on neuronal excitability

We first examined how the loss of $K_v1.1$ and $K_v1.2$ channels affected neuronal excitability. We considered two changes, decreases in D-type conductance (g_{KD}) and decreases in axonal A-type conductance (g_{KA1}). Effects on neuronal excitability were tested in the absence of synaptic inputs in five neuron types: pyramidal neurons in layer II/III (P2/3), IV (P4), V (P5), and VI (P6), and spiny stellate neurons in layer IV (SS4). The results are shown in Figure 3. Decreases in axonal A-type conductance, $g_{KA1,}$ did not significantly affect the excitability of all the tested neurons. They only slightly

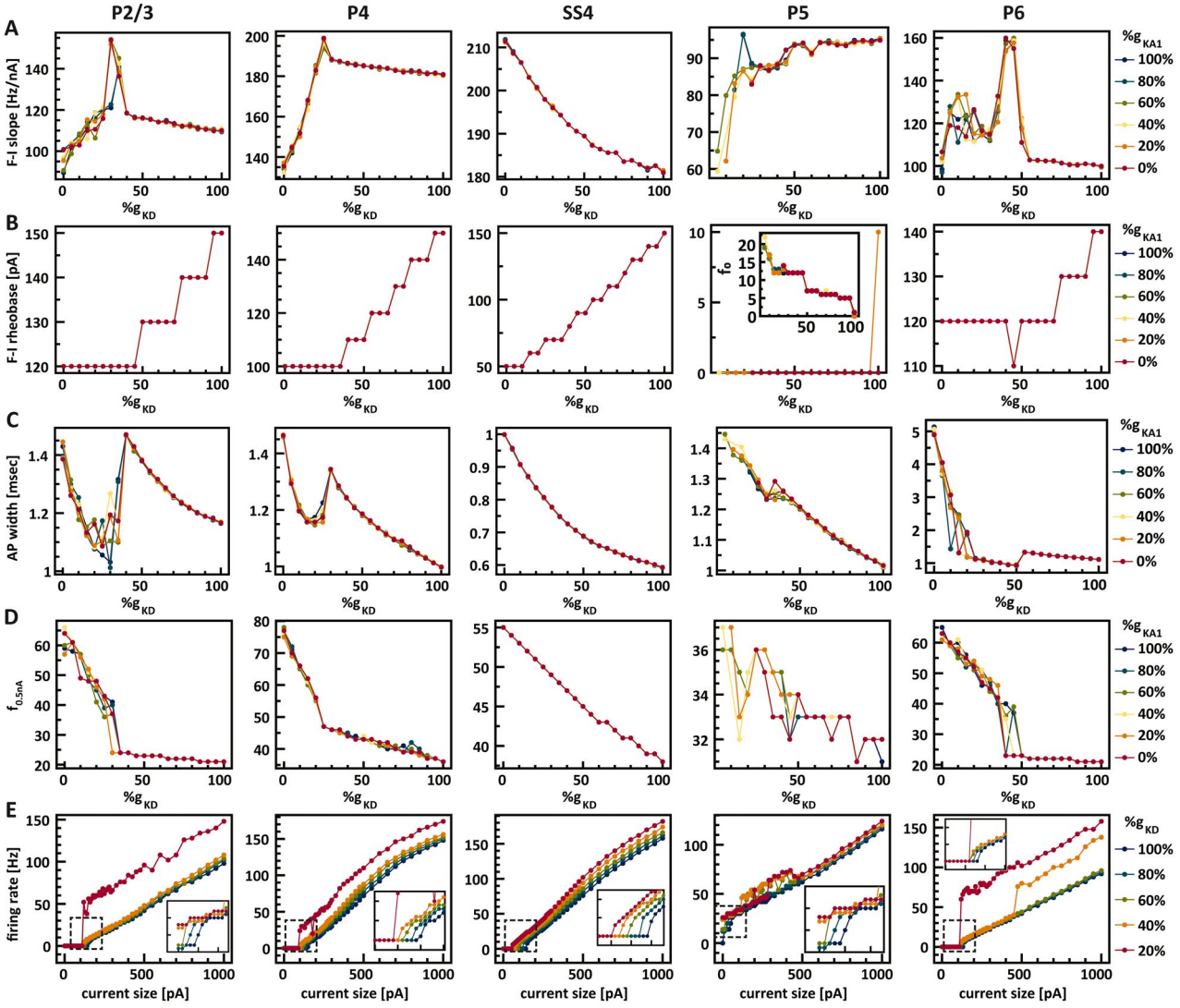

FIGURE 3 Characteristics of neuronal firing with reduced D-type (K_D) and axonal A-type (K_{A1}) potassium currents. Shown are the slopes of F-I curves (A), firing rheobases (B), action potential widths (C), and firing rates with 0.5 nA of currents injected into the soma (D) with reduced peak conductance for D-type (g_{KD}) and axonal A-type (g_{KA1}) potassium currents, and the F-I relationship (E) with reduced g_{KD} produced in the five excitatory cortical neuron types: pyramidal neurons in layer II/III (P2/3, the first column), IV (P4, the second column), V (P5, the fourth column), and VI (P6, the fifth column), and spiny stellate neurons in layer IV (SS4, the third column). The conductance is shown as percentages of the corresponding "normal" values. The inserted figure in (B) displays the spontaneous firing rate for P5 neuron, and the inserted figures in (E) are the magnified pictures for the corresponding indicated regions

changed the firing rates and action potential widths when I_{KD} was extremely low (<70% of its normal value). However, reducing g_{KD} dramatically increased the excitability of all neurons and, g_{KD} modulated the F-I slopes of the neurons. In all neuron types except P5, F-I slopes increased by approximately 10%-20% when D-type conductance was halved, and further reductions decreased the F-I slopes in pyramidal neurons, but not in SS4 neurons. Reducing I_{KD} also lowered firing rheobases. These decreased by 13% in the P2/3, P4, and P6 neurons and by 33% in the SS4 neuron when g_{KD} was halved. The P5 neuron, which is configured to have a low firing rheobase (<10 pA), fired spontaneously with reduced g_{KD}. The spontaneous firing rate (f_0) increased as the conductance decreased. Reducing g_{KD} also widened APs. A 50% reduction in g_{KD} increased AP width by about 20% in all neurons. When g_{KD} was gradually decreased, the firing behaviors of the pyramidal neurons did not change in a continuous fashion. Small to medium reductions in g_{KD} (< 60%) displayed a dominant effect of lowered firing rheobase and increased AP width, whereas increases in firing rate were relatively small. Large g_{KD} reductions displayed more significant effects on firing rates than on firing rheobases or AP width.

Suppression of seizures caused by the loss of $K_v1.1$ and $K_v1.2$ channels requires the effects of reduced g_{KD} to be counteracted. To search for parameters with the potential to reverse the effects of reduced g_{KD}, we systematically varied the conductance of ion channels while decreasing g_{KD}. Reducing persistent sodium conductance (g_{NaP}) compensated for the effects of reduced g_{KD}.

Figure 4 shows neuron firing characteristics when both g_{KD} and g_{NaP} are reduced. F-I slopes decreased for g_{NaP} reductions up to 50%, with further reductions increasing the slopes (refer to Figure 4B). Reduced g_{NaP} also dramatically increased firing rheobases, and significantly reduced the width of APs in all neurons. Herein, AP widths increased with small I_{NaP} reductions and decreased for large I_{NaP} reductions. As such, we estimated the reduction in g_{NaP} required to restore the neuronal changes caused by reductions in g_{KD}. For example, to compensate for a 50% reduction in g_{KD}, less than 25% reduction in g_{NaP} was sufficient to restore the F-I slopes to baseline values, and around 25% reduction was required to restore the rheobases. A further 25% reduction was necessary to restore AP widths in most neuron types except SS4. The required reductions in g_{NaP} varied significantly across neuron types. It was much higher in SS4 neurons, which have the highest density of D-type channels, than in other neuron types.

3.3 | Impacts of K_v1 loss on network dynamics

We incorporated the neuronal changes related to reduced D-type current into the LCM to examine effects on neuronal network dynamics. We first reduced the peak D-type conductance in the axon initial segment of all neurons by 25%, 50%, and 75%. The LCM automatically incorporates the changes in F-I slope, firing rheobase, and firing rate. To simulate effects of widened APs on neurotransmitter release, we also increased the value of neurotransmitter release probability (p_{sy}) in excitatory synapses following the arrival of an AP from 0.6 to 0.8 and 1. The LCM was then used to simulate 20 000 neurons in a 0.5 x 0.5 mm^2 cortical area, reflecting a neuron density similar to that of the cerebral cortex.[29] Local field potentials in the center of the region were generated using the LCM and used to quantify neuronal oscillations. We defined seizure-like activity as LFPs with a mean power spectrum density (PSD) in the 2-20 Hz frequency band exceeding 2.0 μV/Hz; an example is shown in Figure 5B. We measured seizure threshold by systematically varying the conductance of inhibitory synapses. Based on estimates from previous experiments, we set the "normal" conductance to 0.5 nS for AMPA receptors,[30] to 0.4 nS for NMDA receptors,[30] and to 0.8 nS for GABAA receptors.[31] The seizure threshold was defined as the amount of reduction in GABAA receptor conductance (g_{GABAA}) required to induce seizure-like activity. For a neuronal network with "normal" ion channel and receptor function, seizure-like activity was observed when g_{GABAA} was reduced to 0.38 nS, that is, the seizure threshold was 0.42 nS. Reductions in g_{KD} significantly lowered the seizure threshold to 0.36 nS for a 25% reduction, to 0.14 nS for a 50%

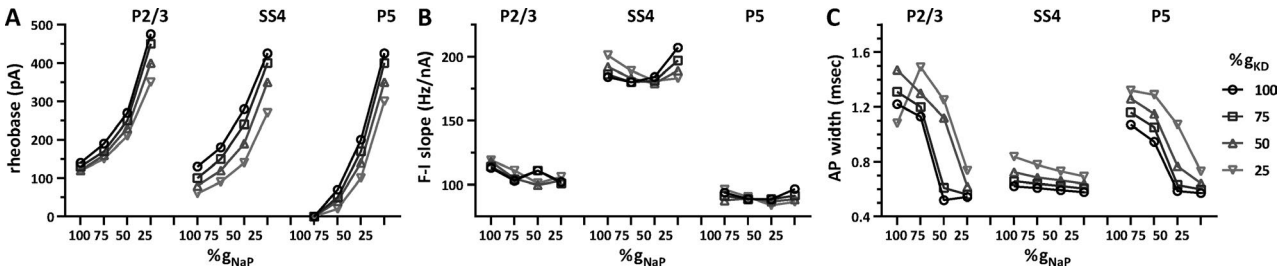

FIGURE 4 Characteristics of neuronal firing with reduced D-type potassium currents (K_D) and persistent sodium currents (Na_P). Shown are the firing rheobases (A), the F-I slopes (B), and action potential width (C) obtained with reduced peak conductance for D-type (g_{KD}) potassium currents and persistent sodium currents (g_{NaP}) in the three excitatory cortical neuron types: pyramidal neurons in layer II/III (P2/3), spiny stellate neurons in layer IV (SS4), pyramidal neurons in layer V (P5). The conductance is shown as percentages of the corresponding "normal" values

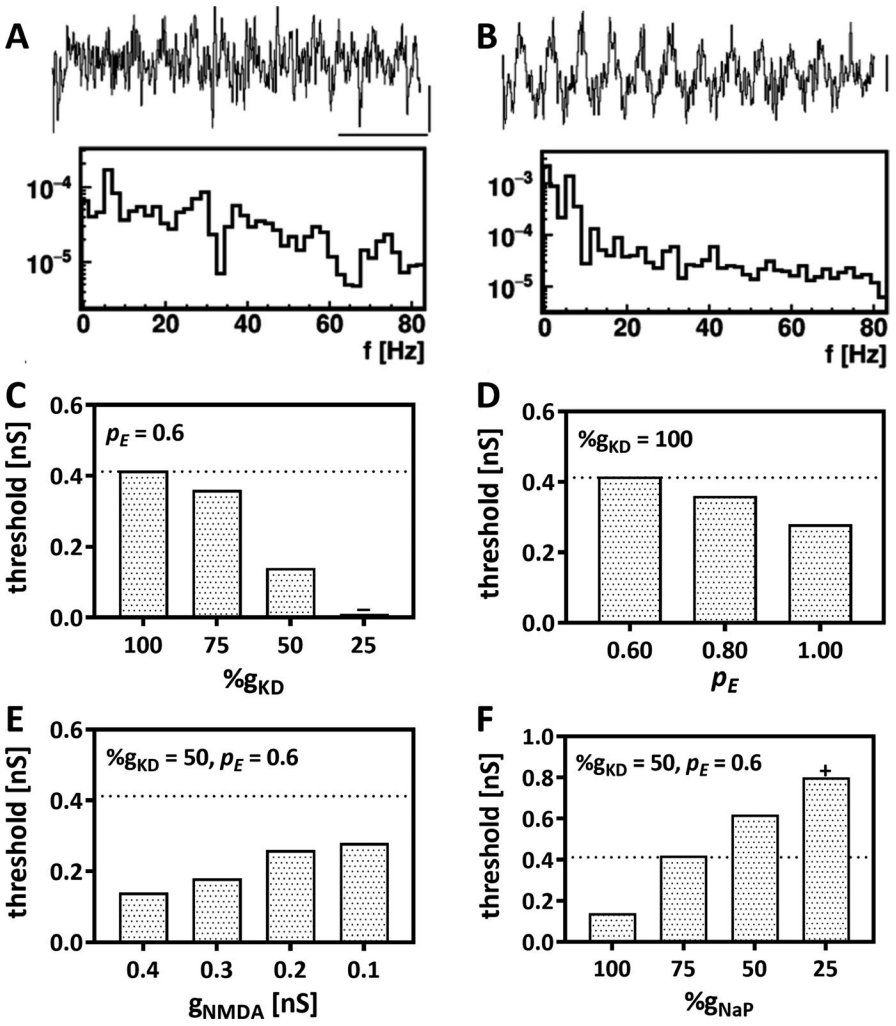

FIGURE 5 Local field potentials (LFPs) and seizure threshold under changes associated with K_v1 and LGI1 mutations and reductions in g_{NaP}. Shown are the examples of "normal" and seizure-like LFPs and their frequency power spectrum density (A and B, scale horizontal bar: 500 ms, vertical bars: 0.1 μV), the GABA thresholds for reduced D-type conductance (g_{KD}, C), increased excitatory neurotransmitter release ratio (p_E, D), reduced conductance of NMDA receptors (g_{NMDA}, E), and persistence sodium conductance (g_{NaP}, F). The conductance is shown as percentages of the corresponding "normal" values. The + sign indicates the seizure threshold higher than the maximum tested value (0.8 nS), and the "−" sign indicates the seizure threshold close to 0

reduction, and to almost zero for a 75% reduction. Increases in p_{sy} also lower the seizure threshold but only modestly. The seizure threshold decreased from 0.42 nS to 0.36 nS when p_{sy} was increased from 0.6 to 0.8, and to 0.28 nS when p_{sy} was set to 1.

We additionally examined two mechanisms that are potentially capable of compensating for the effects of reduced D-type currents: blocking NMDA receptors (g_{NMDA}) or persistent sodium conductance (g_{NaP}). We tested the effects of reducing g_{NMDA} and g_{NaP} in a neuronal network with g_{KD} halved. We found that the seizure threshold increased by only 0.14 nS when g_{NMDA} was decreased from 0.4 to 0.1 nS, but blocking persistent sodium currents significantly increased seizure threshold. A 25% decrease in g_{NaP} was enough to restore seizure threshold to the "normal" value (~0.4 nS), and further g_{NaP} reductions continuously increased seizure threshold.

4 | DISCUSSION

We studied seizure generation in epilepsies associated with mutations affecting K_v1 channels using the LCM simulation platform. $K_v1.1$ and $K_v1.2$ are the most abundant potassium channels in the axon. They activate rapidly at a relatively low voltage compared to other potassium channels, allowing them to be an important determinant of firing thresholds in neurons. Our simulations suggest that decreases in D-type currents lead to lower firing rheobase, higher firing rate, and wider APs. Thereby, decreases in D-type currents are the most important contributing factor to seizure generation in epilepsies associated with loss of function in $K_v1.1$ and $K_v1.2$ channels.

Previous studies on synaptic function in *LGI1* knockout mice have yielded conflicting results with both enhanced excitatory transmission and reduced AMPA receptor function being reported.[6,8–11] Our simulations suggest that enhanced excitatory transmission is likely to be the consequence of a higher level of neurotransmitter release caused by widened APs. Though the loss of the leucine-rich glioma-inactivated 1 protein is associated with reduced expression of AMPA receptor GluA1 subunits, resulting in smaller postsynaptic currents,[4] this effect is outweighed by increases in postsynaptic currents via NMDA receptors. Because inactivation of NMDA

receptors is much slower than that of AMPA receptors, the net effect of *LGI1* loss-of-function mutations is likely to be to lengthen PSCs.

While the effects of manipulations in D-type currents have been studied intensively in many neuron types using the antagonist α-dendrotoxin, K_v1-related A-type currents have been less extensively studied. Previous experiments have found that K_v1.1 and K_v1.4 channels may conduct A-type currents when co-assembling with auxiliary subunits $K_v\beta$1 or $K_v\beta$2.[5,32] Although our simulations suggest that changes in A-type currents do not significantly affect neuronal excitability, further investigation is required to understand their role in neurons.

Based on our findings, we can identify two potential therapeutic targets for treating seizures caused by loss of K_v1.1 and K_v1.2 channels: persistent sodium channels and NMDA receptors. Blocking persistent sodium channels can reverse the effects of diminished D-type currents and restore the firing rheobase and AP width, and NMDA receptor antagonism reduces the changes in excitatory postsynaptic currents due to increased glutamate release. In our model, both these effects can suppress seizures caused by loss of K_v1.1 and K_v1.2 channel functions. We propose that riluzole could be repurposed to treat epilepsy caused by *LGI1*, *KCNA1,* or *KCNA2* loss-of-function mutations. By blocking persistent sodium currents[33,34] but not transient sodium currents, riluzole does not have the same side effect profile as other antiepileptic drugs acting on the sodium channel, such as carbamazepine. Besides, riluzole may increase D-type currents by dramatically slowing down the inactivation of K_v1.4 channels.[35,36] At around 100 μmol/L concentrations, the inactivation time constant of K_v1.4 channels is prolonged to more than 680 ms and converts the A-type currents to D-type currents. Furthermore, riluzole also blocks NMDA receptors noncompetitively[37] and increases Ca^{2+}-activated potassium currents.[38] The four effects are all desirable for treating epilepsy associated with loss of K_v1.1 and K_v1.2 channels. Our simulation suggests that a 25% reduction in persistent sodium currents is sufficient to restore the seizure threshold of neuronal network with halved D-type currents. A previous experiment found 10 μmol/L of riluzole almost completely blocked the persistent sodium currents, and a 25% reduction requires about 1 μmol/L of riluzole,[35] which corresponds to the plasma concentrations of riluzole achieved at the suggested therapeutic dose (2 × 50 mg/d).[39]

Sodium currents in neurons are known to contain many components with distinctive biophysical features. Our simulations modeled both transient and persistent sodium currents. Rapid-activating, rapid-inactivating transient sodium currents account for >90% of the total sodium currents in neurons. They are responsible for the depolarization phase of action potentials and are thus a determinant of firing thresholds and action potential shapes. Rapid-activating, slow-inactivating persistent sodium currents comprise up to 10% of the total sodium currents. They typically activate at subthreshold membrane potentials and enhance repetitive action potential firing and synaptic transmission.[40] Another type of sodium current is the "resurgent current" which is found in ~20, predominantly inhibitory, neuron types. Resurgent currents appear when neurons are repolarized after prolonged depolarization. They are reported to promote spontaneous firing and high-frequency firing of inhibitory neurons and may be a promising antiepileptic therapeutic target.[41,42] A computer model that includes the unique activation features of resurgent currents is still to be developed.

Seizures caused by loss of D-type currents may also be treated using activators of voltage-gated potassium channels. A group of compounds shown to enhance potassium currents through K_v1.1 channels by delaying inactivation of the channels may be a potential treatment for K_v1 channel-related epilepsy.[43] Further work investigating specific pharmacological activators or inhibitors of D-type currents that can be potentially tailored for this application is imperative. Activators of M-type currents could also be used to treat seizures. M-type currents, which are conducted by K_v7.2 and K_v7.3 channels, share many characters with D-type currents. For example, they both activate at a relatively low voltage (around −45 mV), M-type currents are non-inactivating, and D-type currents are slowly inactivating (with a time constant of 1 second), and they are both abundant in the axon initial segment. Agents that enhance M-type currents include flupirtine and its analogue retigabine.[44–48] Both negatively shift the activation threshold of K_v7.2 and K_v7.3 channels,[49,50] leading to significant increases in M-type currents during resting and depolarization states.[50]

ACKNOWLEDGMENTS

This work was supported by Australian Research Council (ARC) under Discovery Projects funding scheme (project number DP150104771). We wish to acknowledge The University of Queensland's Research Computing Centre (RCC) for its support in this research.

CONFLICT OF INTERESTS

Neither of the authors has any conflict of interest to disclose. We confirm that we have read the Journal's position on issues involved in ethical publication and affirm that this report is consistent with those guidelines.

ORCID

Jiaxin Du https://orcid.org/0000-0003-0620-2300
Viktor Vegh https://orcid.org/0000-0002-4310-1421
David C. Reutens https://orcid.org/0000-0002-1652-9369

REFERENCES

1. Villa C, Combi R. Potassium channels and human epileptic phenotypes: an updated overview. Front Cell Neurosci. 2016;10:81.
2. Monaghan MM, Trimmer JS, Rhodes KJ. Experimental localization of Kv1 family voltage-gated K+ channel alpha and beta subunits in rat hippocampal formation. J Neurosci. 2001;21:5973–83.
3. Inda MC, DeFelipe J, Munoz A. Voltage-gated ion channels in the axon initial segment of human cortical pyramidal cells and their relationship with chandelier cells. Proc Natl Acad Sci U S A. 2006;103:2920–5.
4. Petit-Pedrol M, Sell J, Planaguma J, Mannara F, Radosevic M, Haselmann H, et al. LGI1 antibodies alter Kv1.1 and AMPA receptors changing synaptic excitability, plasticity and memory. Brain. 2018;141:3144–59.
5. Seagar M, Russier M, Caillard O, Maulet Y, Fronzaroli-Molinieres L, De San FM, et al. LGI1 tunes intrinsic excitability by regulating the density of axonal Kv1 channels. Proc Natl Acad Sci U S A. 2017;114:7719–24.
6. Boillot M, Lee CY, Allene C, Leguern E, Baulac S, Rouach N. LGI1 acts presynaptically to regulate excitatory synaptic transmission during early postnatal development. Sci Rep. 2016;6:21769.
7. Lovero KL, Fukata Y, Granger AJ, Fukata M, Nicoll RA. The LGI1-ADAM22 protein complex directs synapse maturation through regulation of PSD-95 function. Proc Natl Acad Sci U S A. 2015;112:E4129–E4137.
8. Ohkawa T, Fukata Y, Yamasaki M, Miyazaki T, Yokoi N, Takashima H, et al. Autoantibodies to epilepsy-related LGI1 in limbic encephalitis neutralize LGI1-ADAM22 interaction and reduce synaptic AMPA receptors. J Neurosci. 2013;33:18161–74.
9. Fukata Y, Lovero KL, Iwanaga T, Watanabe A, Yokoi N, Tabuchi K, et al. Disruption of LGI1-linked synaptic complex causes abnormal synaptic transmission and epilepsy. Proc Natl Acad Sci U S A. 2010;107:3799–804.
10. Fukata Y, Adesnik H, Iwanaga T, Bredt DS, Nicoll RA, Fukata M. Epilepsy-related ligand/receptor complex LGI1 and ADAM22 regulate synaptic transmission. Science. 2006;313:1792–5.
11. Higgs MH, Spain WJ. Kv1 channels control spike threshold dynamics and spike timing in cortical pyramidal neurones. J Physiol. 2011;589:5125–42.
12. Du J, Vegh V, Reutens DC. The laminar cortex model: a new continuum cortex model incorporating laminar architecture. PLoS Comput Biol. 2012;8:e1002733.
13. Du J, Vegh V, Reutens DC. Small changes in synaptic gain lead to seizure-like activity in neuronal network at criticality. Sci Rep. 2019;9:1097.
14. Gentet LJ, Stuart GJ, Clements JD. Direct measurement of specific membrane capacitance in neurons. Biophys J. 2000;79:314–20.
15. Traub RD, Buhl EH, Gloveli T, Whittington MA. Fast rhythmic bursting can be induced in layer 2/3 cortical neurons by enhancing persistent Na+ conductance or by blocking BK channels. J Neurophysiol. 2003;89:909–21.
16. Hay E, Hill S, Schurmann F, Markram H, Segev I. Models of neocortical layer 5b pyramidal cells capturing a wide range of dendritic and perisomatic active properties. PLoS Comput Biol. 2011;7:e1002107.
17. Wang XJ. Calcium coding and adaptive temporal computation in cortical pyramidal neurons. J Neurophysiol. 1998;79:1549–66.
18. Jahr CE, Stevens CF. A quantitative description of NMDA receptor-channel kinetic behavior. J Neurosci. 1990;10:1830–7.
19. Nunez PL, Srinivasan R. Electric Fields of the Brain: The Neurophysics of EEG. Oxford; New York: Oxford University Press, 2006.
20. Druckmann S, Banitt Y, Gidon A, Schurmann F, Markram H, Segev I. A novel multiple objective optimization framework for constraining conductance-based neuron models by experimental data. Front Neurosci. 2007;1:7–18.
21. Markram H, Muller E, Ramaswamy S, Reimann MW, Abdellah M, Sanchez CA, et al. Reconstruction and simulation of neocortical microcircuitry. Cell. 2015;163:456–92.
22. Roeper J, Lorra C, Pongs O. Frequency-dependent inactivation of mammalian A-type K+ channel KV1.4 regulated by Ca2+/calmodulin-dependent protein kinase. J Neurosci. 1997;17:3379–91.
23. Mendonca PR, Vargas-Caballero M, Erdelyi F, Szabo G, Paulsen O, Robinson HP. Stochastic and deterministic dynamics of intrinsically irregular firing in cortical inhibitory interneurons. Elife. 2016;5:e16475.
24. Hines ML, Carnevale NT. The NEURON simulation environment. Neural Comput. 1997;9:1179–209.
25. Johnston D, Wu SM. Foundations of Cellular Neursophysiology. Cambridge, MA: MIT Press, 1995.
26. Guan D, Armstrong WE, Foehring RC. Electrophysiological properties of genetically identified subtypes of layer 5 neocortical pyramidal neurons: Ca(2)(+) dependence and differential modulation by norepinephrine. J Neurophysiol. 2015;113:2014–32.
27. Degenetais E, Thierry AM, Glowinski J, Gioanni Y. Electrophysiological properties of pyramidal neurons in the rat prefrontal cortex: an in vivo intracellular recording study. Cereb Cortex. 2002;12:1–16.
28. Nowak LG, Azouz R, Sanchez-Vives MV, Gray CM, McCormick DA. Electrophysiological classes of cat primary visual cortical neurons in vivo as revealed by quantitative analyses. J Neurophysiol. 2003;89:1541–66.
29. Beaulieu C, Colonnier M. The number of neurons in the different laminae of the binocular and monocular regions of area 17 in the cat, Canada. J Comp Neurol. 1983;217:337–44.
30. Sarid L, Feldmeyer D, Gidon A, Sakmann B, Segev I. Contribution of intracolumnar layer 2/3-to-Layer 2/3 excitatory connections in shaping the response to whisker deflection in rat barrel cortex. Cereb Cortex. 2015;25:849–58.
31. Hoffmann JHO, Meyer HS, Schmitt AC, Straehle J, Weitbrecht T, Sakmann B, et al. Synaptic conductance estimates of the connection between local inhibitor interneurons and pyramidal neurons in layer 2/3 of a cortical column. Cereb Cortex. 2015;25:4415–29.
32. Chen SH, Fu SJ, Huang JJ, Tang CY. The episodic ataxia type 1 mutation I262T alters voltage-dependent gating and disrupts protein biosynthesis of human Kv1.1 potassium channels. Sci Rep. 2016;6:19378.
33. Spadoni F, Hainsworth AH, Mercuri NB, Caputi L, Martella G, Lavaroni F, et al. Lamotrigine derivatives and riluzole inhibit Ina, P in cortical neurons. Neuroreport. 2002;13:1167–70.
34. Urbani A, Belluzzi O. Riluzole inhibits the persistent sodium current in mammalian CNS neurons. Eur J Neurosci. 2000;12:3567–74.
35. Ahn HS, Choi JS, Choi BH, Kim MJ, Rhie DJ, Yoon SH, et al. Inhibition of the cloned delayed rectifier K+ channels, Kv1.5 and Kv3.1, by riluzole. Neuroscience. 2005;133:1007–19.
36. Xu L, Enyeart JA, Enyeart JJ. Neuroprotective agent riluzole dramatically slows inactivation of Kv1.4 potassium channels by a voltage-dependent oxidative mechanism. J Pharmacol Exp Ther. 2001;299:227–37.

37. Lamanauskas N, Nistri A. Riluzole blocks persistent Na+ and Ca2+ currents and modulates release of glutamate via presynaptic NMDA receptors on neonatal rat hypoglossal motoneurons in vitro. Eur J Neurosci. 2008;27:2501–14.
38. Wang YJ, Lin MW, Lin AA, Wu SN. Riluzole-induced block of voltage-gated Na+ current and activation of BKCa channels in cultured differentiated human skeletal muscle cells. Life Sci. 2008;82:11–20.
39. Le Liboux A, Lefebvre P, Le Roux Y, Truffinet P, Aubeneau M, Kirkesseli S, et al. Single- and multiple-dose pharmacokinetics of riluzole in white subjects. J Clin Pharmacol. 1997;37:820–7.
40. Stafstrom CE. Persistent sodium current and its role in epilepsy. Epilepsy Curr. 2007;7:15–22.
41. So EC, Wu S-N, Lo Y-C, Su K. Differential regulation of tefluthrin and telmisartan on the gating charges of INa activation and inactivation as well as on resurgent and persistent INa in a pituitary cell line (GH3). Toxicol Lett. 2018;285:104–12.
42. Hong H, Lu T, Wang XY, Wang Y, Sanchez JT. Resurgent sodium current promotes action potential firing in the avian auditory brainstem. J Physiol. 2018;596:423–43.
43. Lu Q, Peevey J, Jow F, Monaghan MM, Mendoza G, Zhang H, et al. Disruption of Kv1.1 N-type inactivation by novel small molecule inhibitors (disinactivators). Bioorg Med Chem. 2008;16:3067–75.
44. Wua YJ, Dworetzky SI. Recent developments on KCNQ potassium channel openers. Curr Med Chem. 2005;12:453–60.
45. Blackburn-Munro G, Jensen BS. The anticonvulsant retigabine attenuates nociceptive behaviours in rat models of persistent and neuropathic pain. Eur J Pharmacol. 2003;460:109–16.
46. Wu YJ, Boissard CG, Greco C, Gribkoff VK, Harden DG, He H, et al. (S)-N-[1-(3-morpholin-4-ylphenyl)ethyl]- 3-phenylacrylamide: an orally bioavailable KCNQ2 opener with significant activity in a cortical spreading depression model of migraine. J Med Chem. 2003;46:3197–200.
47. Ilyin V, Carlin KP, Hodges DD, Robeldo S, Woodward RM. Flupirtine: A Positive Modulator of Heteromeric KCNQ2/Q3 Channels. Program No. 785.10. 2002 Neuroscience Meeting Planner. Orlando, FL: Society for Neuroscience, 2002.
48. Brown DA, Passmore GM. Neural KCNQ (Kv7) channels. Br J Pharmacol. 2009;156:1185–95.
49. Tatulian L, Brown DA. Effect of the KCNQ potassium channel opener retigabine on single KCNQ2/3 channels expressed in CHO cells. J Physiol. 2003;549:57–63.
50. Wladyka CL, Kunze DL. KCNQ/M-currents contribute to the resting membrane potential in rat visceral sensory neurons. J Physiol. 2006;575:175–89.

SUPPORTING INFORMATION

Additional supporting information may be found online in the Supporting Information section.

How to cite this article: Du J, Vegh V, Reutens DC. Persistent sodium current blockers can suppress seizures caused by loss of low-threshold D-type potassium currents: Predictions from an in silico study of K_v1 channel disorders. *Epilepsia Open*. 2020;5:86–96. https://doi.org/10.1002/epi4.12379